

limit the degree to which the femur can act in a vertical plane without contacting the pelvis. This contrasts with modern bipedal lizards in which the large trochanter is adjacent to and directly below the proximal head and would be forced against the ventral acetabular rim during adduction of the femur, levering the head from the socket (10–12, 14). With increasing speeds during bipedal running in lizards, the femur may approach a vertical orientation at footfall, but this is accomplished by pelvic roll rather than by adduction (15). Although the acetabulum is not exposed in *E. cursoris*, a partial pelvis of *B. striatus* does show a strong dorsal acetabular rim that would have facilitated a near-vertical femoral orientation (4).

The forelimb of *Eudibamus* also possesses several features that can be interpreted as adaptations to parasagittal locomotion: (i) the humerus is elongate and slender but has retained a large deltopectoral crest, (ii) the carpus is compact, and (iii) the digits of the hand are greatly elongated. The overall elongation of the forelimb and manus indicate that *Eudibamus* was probably capable of parasagittal quadrupedal locomotion until speeds were reached that required bipedalism. As *Eudibamus* was herbivorous, based on the typical bolosaurid dental and mandibular morphology (7), it likely used sprinting speeds to escape predators.

Although small in size and mainly repre-

sented in the fossil record by fragmentary remains, bolosaurid parareptiles (Fig. 4) are unusual among amniotes in achieving a wide Laurasian distribution early in the Permian (20), which includes the United States, Germany, southern Russia, and China (4–6). Perhaps this precocious dispersal and early success were related to the unique combination of bipedalism and herbivory.

References and Notes

1. R. R. Reisz, *Trends Ecol. Evol.* **12**, 218 (1997).
2. Etymology: Greek *eu*, meaning original or primitive, and *dibamos*, meaning on two legs; Latin *cursoris*, meaning runner. Holotype: MNG (Museum der Natur Gotha, Germany) 8852. Horizon and locality: Lower Permian Tambach Formation, Upper Rotliegend, in the Broecker quarry locality of the middle part of the Thuringian Forest near the village of Tambach-Dietharz and about 20 km south of Gotha, Thuringia, central Germany. Diagnosis: Small bolosaurid parareptile distinguished by the presence of long, narrow, boomerang-shaped postfrontal; three premaxillary teeth, rather than two; interpterygoid vacuity narrow, rather than closed; and dorsal lamina of maxilla low.
3. D. A. Eberth, D. S. Berman, S. S. Sumida, H. Hopf, *Palaio* **15**, 293 (2000).
4. D. M. S. Watson, *Bull. Mus. Comp. Zool.* **111**, 299 (1954).
5. M. F. Ivachnenko, G. I. Tverdokhlebova, *Paleontol. J.* **1987**, 93 (1987).
6. J. Li, Z. Cheng, *Palaeontol.* **33**, 17 (1995).
7. N. Hotton III, E. C. Olson, R. Beerbower, in *Amniote Origins*, S. S. Sumida, K. L. M. Martin, Eds. (Academic Press, San Diego, CA, 1997), pp. 207–264.
8. R. L. Carroll, *Vertebrate Paleontology and Evolution* (Freeman, New York, 1998).
9. R. L. Carroll, P. Thompson, *J. Paleontol.* **56**, 1 (1982).
10. R. C. Snyder, *Copeia* **1949**, 129 (1949).
11. R. C. Snyder, *Am. J. Anat.* **95**, 1 (1954).
12. R. C. Snyder, *Am. Zool.* **2**, 191 (1962).
13. D. J. Irschick, B. C. Jayne, *J. Exp. Biol.* **202**, 1047 (1999).
14. R. C. Snyder, *Copeia* **1952**, 64 (1952).
15. C. L. Fieler, B. C. Jayne, *J. Exp. Biol.* **201**, 609 (1998).
16. F. E. Novas, *J. Vertebr. Paleontol.* **16**, 723 (1996).
17. J. M. Clark, J. A. Hopson, R. Hernandez, D. E. Fastovsky, M. Montellano, *Nature* **379**, 886 (1998).
18. S. C. Rawcastle, *J. Zool. London* **191**, 147 (1980).
19. R. Holmes, *J. Morphol.* **152**, 101 (1977).
20. D. S. Berman, S. S. Sumida, R. E. Lombard, in *Amniote Origins: Completing the Transition to Land*, S. S. Sumida, K. L. M. Martin, Eds. (Academic Press, San Diego, CA, 1997), chap. 4, pp. 85–139.
21. R. R. Reisz, *Occas. Pap. Mus. Nat. Hist. Univ. Kansas* **7**, 1 (1981).
22. R. Carroll, *J. Paleontol.* **43**, 151 (1969).
23. M. Heaton, R. R. Reisz, *J. Paleontol.* **54**, 13 (1980).
24. M. Laurin, R. R. Reisz, *Biol. J. Linn. Soc.* **113**, 165 (1995).
25. S. Modesto, *Palaeont. Afr.* **36**, 15 (2000).
26. A. S. Romer, L. I. Price, *Spec. Pap. Geol. Soc. Am.* **28**, 1 (1941).
27. R. F. Ewer, *Philos. Trans. R. Soc. London Ser. B* **248**, 379 (1965).
28. We thank two anonymous reviewers and H.-D. Sues and S. Modesto for their helpful suggestions and R. Blob and D. Dilkes for discussions on bipedal locomotion. Supported by grants from the National Geographic Society, the Natural Sciences and Engineering Research Council of Canada, the Edward O'Neil Endowment Fund and M. Graham Netting Research Fund, the Carnegie Museum of Natural History, and the Deutsche Forschungsgemeinschaft.

23 August 2000; accepted 23 September 2000

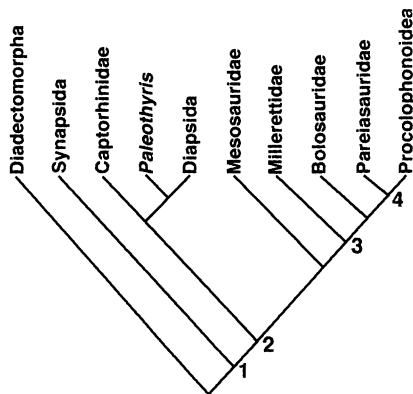


Fig. 4. Cladogram of Paleozoic amniotes, illustrating the single most parsimonious pattern of relationships from a PAUP version 3.1.1 analysis (D. Swofford, Laboratory of Molecular Systematics, Smithsonian Institution, 1993), based on previously published data matrices (24, 25) except for the inclusion of bolosaurids. The tree length is 225 steps, with a consistency index of 0.809 and a retention index of 0.672. Major clades are designated as follows: 1, Amniota; 2, Reptilia; 3, Parareptilia; and 4, Procolophonidea. It is the anatomy of *E. cursoris* that has allowed us to determine for the first time that bolosaurids are parareptiles and the sister taxon of Procolophonidea. The high position of bolosaurids within parareptiles is unexpected, as the bolosaurids are the oldest known members of this clade, with a fossil record extending to the base of the Permian. However, this finding is consistent with recent phylogenetic data that indicate the presence of long ghost lineages for parareptiles (25).

A Kingdom-Level Phylogeny of Eukaryotes Based on Combined Protein Data

Sandra L. Baldauf,^{1*} A. J. Roger,²
I. Wenk-Siefert,^{3†} W. F. Doolittle²

Current understanding of the higher order systematics of eukaryotes relies largely on analyses of the small ribosomal subunit RNA (SSU rRNA). Independent testing of these results is still limited. We have combined the sequences of four of the most broadly taxonomically sampled proteins available to create a roughly parallel data set to that of SSU rRNA. The resulting phylogenetic tree shows a number of striking differences from SSU rRNA phylogeny, including strong support for most major groups and several major supergroups.

SSU rRNA sequences constitute the single most comprehensive database available for phylum-level systematics (1–4). These data de-

scribe the eukaryotes as a series of deeply diverging lineages branching successively toward a dense unresolved cluster [the so-called eukaryote crown (5)]. Because the latter include the majority of eukaryotes, this has led to suggestions that most major eukaryote taxa arose in a single explosive radiation (5, 6), and, together with poor resolution in many protein-based phylogenies, to speculation that relationships among these taxa may never be resolved (6). Although phylogenies of protein genes and rRNAs often conflict, currently available protein data are plagued by uneven taxonomic sampling, wide disparities in evolutionary rates

¹Department of Biology, University of York, Heslington, York, YO10 5DD, UK. ²Canadian Institute for Advanced Research—Program in Evolutionary Biology, Department of Biochemistry and Molecular Biology, Dalhousie University, Halifax, Nova Scotia, B3H 4H7 Canada. ³Institut für Pflanzenbiologie, Universität Zürich, CH-8008 Zürich, Switzerland.

*To whom correspondence should be addressed. E-mail: slb14@york.ac.uk

†Present address: Kuehried-Weg 28, CH-8050 Zurich, Switzerland.

REPORTS

among lineages, and/or inadequate characterization. The first two phenomena tend to cause the artifactual clustering of long branches (7), whereas the latter may result in failure to detect taxonomically confounding gene paralogies or lateral gene transfers.

We attempted to overcome these problems and to create a well-resolved parallel phylogeny to that of SSU rRNA by combining the deduced amino acid sequences of four protein-

encoding genes. The encoded proteins— α -tubulin, β -tubulin, actin, and elongation factor 1- α (EF-1 α)—are the only proteins currently available with sufficient length, breadth of sampling, and level of sequence conservation to test ancient evolutionary relationships (8). These proteins are all ~400 amino acids long, with ≥ 65 to 70% identity among all taxa, and are therefore expected to contribute similarly in combined analyses.

All taxa with sequence data for a minimum of three of these proteins were included, plus several key taxa with sequence data from only one or two proteins (9). Major groups represented by only a single taxon or set of closely related taxa were excluded, except for the glaucophyte and rhodophyte algae because of current interest in these taxa (10). Including a substantial amount of missing data limited the choice of phylogenetic method used

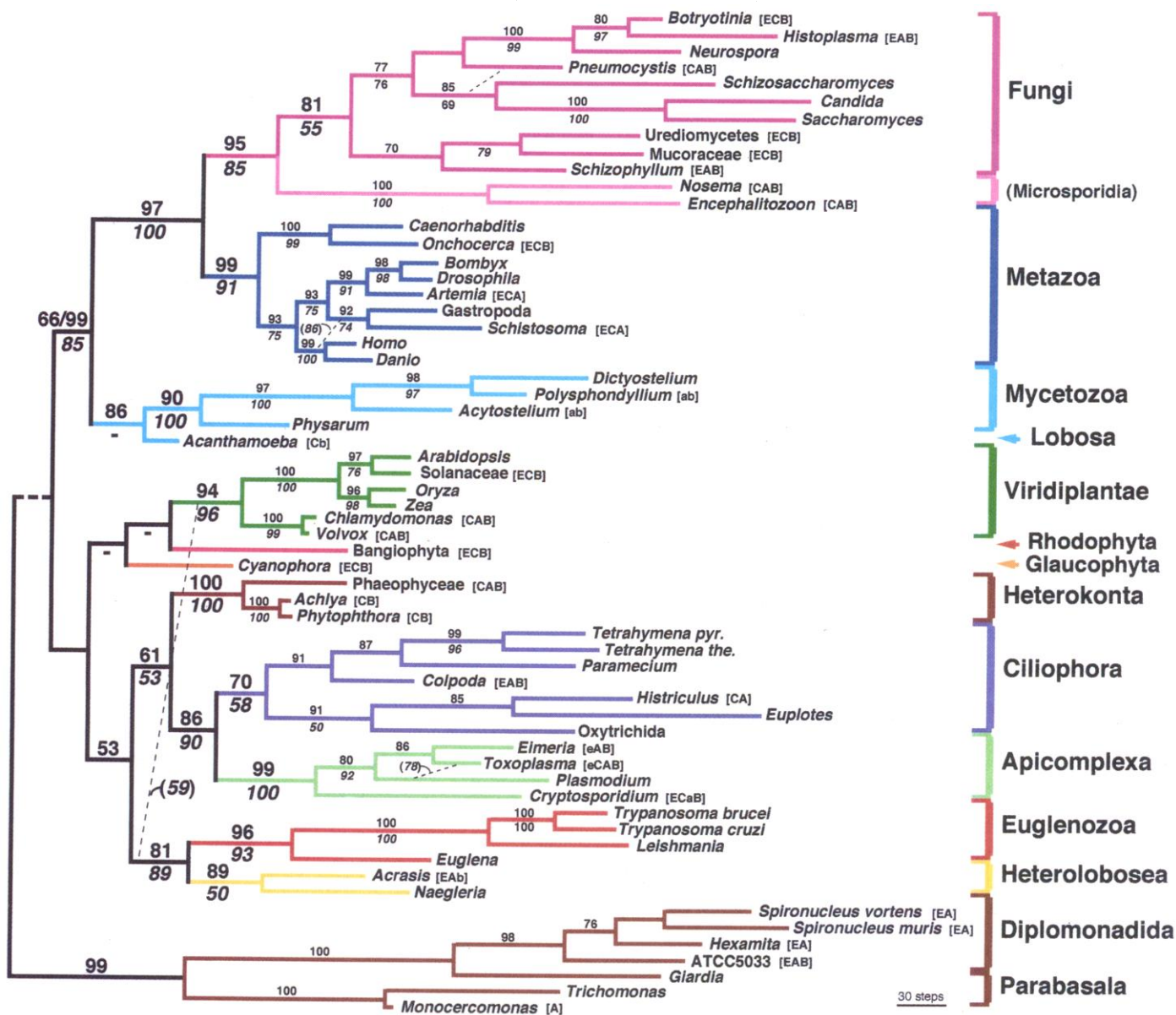


Fig. 1. A kingdom-level phylogeny of eukaryotes, based on combined protein sequences. The tree shown is one of two shortest trees found by parsimony analysis of concatenated EF-1 α , actin, α -tubulin, and β -tubulin amino acid sequences (44). The tree is 5056 steps long with branches drawn to scale as indicated (43, 45). Bootstrap values $> 50\%$ are shown above and below the lines, respectively, for amino acid parsimony (aaBP) and maximum likelihood analyses of second codon-position nucleotides (ntBP). Parenthesis indicate the aaBP for the grouping of animals + fungi plus lobosa + mycetozoa in analyses omitting Bangiophyceae and *Cyanophora* (see text). Dashes (–) below lines indicate nodes not tested in the ntBP analyses shown [Bangio-

phyceae, *Cyanophora*, and *Acanthamoeba* omitted; see text (29)]. For taxa with missing data, the sequences used are indicated in brackets to the right of taxon names in uppercase and lowercase letters for complete and partial sequences, respectively (E = EF-1 α , C = actin, A = α -tubulin, B = β -tubulin). The lowest common taxonomic designation is given for sequences combined from different taxa. The shortest trees differ only in their placement of *Pneumocystis*, as shown by the thin dashed line; all other slanting dashed lines indicate alternative groupings found with ntBP $> 50\%$. The horizontal dashed line (left center) indicates tentative placement of the Diplomonadida and Parabasalia (46).

(11) to unweighted parsimony (12), with results confirmed by nucleotide-level maximum likelihood (13). The accuracy of amino acid parsimony with these data is shown by previous analyses excluding taxa with missing entries, where neighbor-joining distance and protein

maximum likelihood found equivalent results to parsimony (8).

Phylogenetic analysis of the concatenated, deduced amino acid sequences of four protein-encoding genes produces a highly resolved phylogenetic tree including 14 higher order

eukaryote taxa (Figs. 1 and 2A). Forty-nine of a total of 58 nodes receive bootstrap percentage (BP) support of 75% or greater at the amino acid level [$\sim 95\%$ probable accuracy (14)], slightly lower in some cases at the nucleotide level (Fig. 1). Of the 11 higher order taxa with multiple representatives, all are reconstructed as monophyletic; all but one are supported by $>89\%$ bootstrap at the amino acid level (aaBP, Fig. 1) and all but two by $>85\%$ bootstrap at the nucleotide level (ntBP, Fig. 1). Only the ciliates receive a relatively low aaBP of 70% (58% ntBP, Fig. 1), likely due to their fast evolutionary rates for both EF-1 α (15) and actin (16). Of these 11 major taxa, only the Fungi + Microsporidia and the Mycetozoa are controversial.

The Microsporidia were long classified as early-branching eukaryotes on the basis of SSU rRNA trees [e.g., (2–4)], which is further supported by early analyses of EF-1 α , elongation factor 2 (EF-2), and large subunit (LSU) rRNA [reviewed in (17)]. However, the strong placement of these taxa with fungi in our tree (95% aaBP, 85% ntBP, Fig. 1; Fig. 2A, node 2) is also found in trees of α -tubulin, β -tubulin, RNA polymerase II largest subunit (RPB1), valyl-tRNA synthetase, and the TATA box binding protein (Fig. 2B) (17). Microsporidial EF-1 α 's also encode an insertion diagnostic of animals and fungi (8, 17, 18). Reanalyses of EF-1 α , EF-2, and SSU and LSU rRNA suggest that the early branching of Microsporidia in these trees is an artifact of their accelerated evolutionary rates for these genes [reviewed in (17)].

The long-standing controversy over the monophyly of the Mycetozoa (Fig. 2A, node 5) has been fueled by the failure of these taxa to branch together in most SSU [(3, 4), but see (2)] and LSU (19) rRNA trees. However, the strong placement of these taxa together in our tree (90% aaBP, 100% ntBP, Fig. 1) is also seen with α -tubulin, β -tubulin, actin, and EF-1 α [with the latter case also including protostelid slime molds (Fig. 2B) (20)]. All Mycetozoa also produce morphologically similar, quasi-multicellular fruiting bodies (21). Therefore, the apparent unrelatedness of myxogastrid (plasmodial, e.g., *Physarum*) and cellular (e.g., *Dictyostelium*) slime mold rRNA sequences (Fig. 2B) may be an artifact of their fast evolutionary rates and oppositely skewed G+C nucleotide contents (3).

It is at the “super-taxon” level especially that the combined data show markedly greater resolution than any single-gene phylogeny (Figs. 1 and 2B). This includes a new protistan supertaxon of Euglenozoa + Heterolobosea (the Discicristata). Four other higher level associations receive $>86\%$ aaBP support ($>85\%$ ntBP, Fig. 1): Animalia + Fungi (opisthokonts), Ciliophora + Apicomplexa (Alveolata), Mycetozoa + Lobosa (Amoebo-

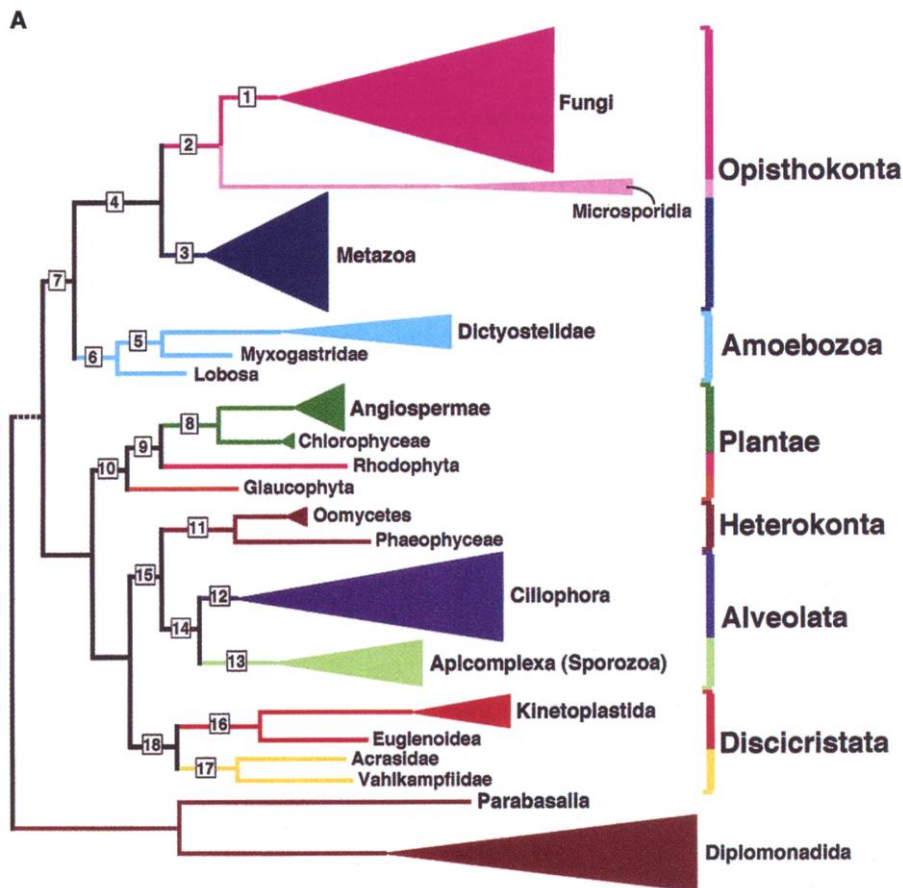
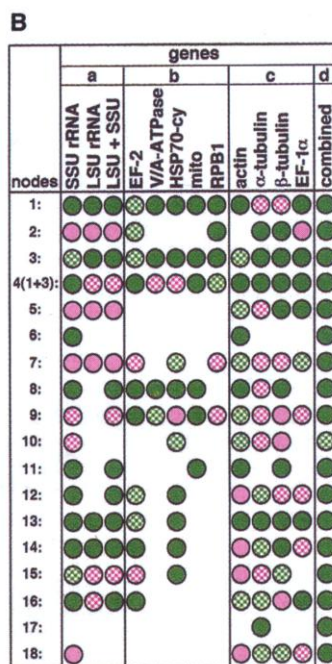


Fig. 2. Single-gene phylogenies support subsets of the combined protein tree. (A) A summary of the tree in Fig. 1 is shown with supergroups indicated beside brackets to the right. Multi-taxon represented clusters are given as triangles, with height proportional to number of taxa and width proportional to averaged overall branch length (1) compensated for missing data (47). (B) Published support for the numbered nodes in (A) is shown for commonly used molecular phylogenetic markers grouped as (a) ribosomal RNAs, (b) proteins not used in the current analysis, (c) proteins used in the current analysis, and (d) the combined data (Fig. 1). These markers are, from left to right, SSU [SSU rRNA (1–4)], LSU [LSU rRNA (19)], LSU + SSU [combined LSU and SSU rRNA (48)], EF-2 (10), V/A-ATPases [vacuolar ATPases (49)], HSP70-cy [cytosolic 70-kD heat shock protein (50)], mito [combined mitochondrial proteins (51)], RPB1 (52), actin (8, 16, 53), α -tubulin (8, 54), β -tubulin (8, 54), EF-1 α (15, 20), and combined (Fig. 1). Rejected nodes are indicated in pink and accepted nodes in green, with checked circles indicating BP $< 70\%$ and solid circles indicating BP $> 70\%$.



REPORTS

zoa), and an even higher level clustering of Amoebozoa + opisthokonts. Two further supertaxa are suggested with moderate or weak support, respectively: Alveolata + Heterokonta (chromalveolates) and a holophyletic Plantae (Fig. 1). In contrast, most individual molecules, including SSU rRNA, reconstruct less than half of these groups (Fig. 2B).

Combined protein data strongly support a cluster of Euglenozoa + Heterolobosea (81% aaBP, 89% ntBP, Fig. 1; Fig. 2A, node 18). The only previous molecular phylogenetic support for this group comes from analyses of β -tubulin, particularly with limited taxa and semi-constrained branches (22). However, other data are suggestive; these taxa tend to branch near each other in trees of α -tubulin and SSU rRNA (Fig. 2B) and, at least in the case of *Acrasis*, EF-1 α (18). A possible close evolutionary relationship between euglenozoans and heteroloboseans was proposed by Patterson and others on the basis of their shared possession of discoidally shaped mitochondrial cristae (23), hence the term “discicristates,” later formalized to Discicristata (24). However, this mitochondrial morphology is reported in several enigmatic protists, i.e., *Malawimonas*, *Nuclearia*, *Stephanopogon*, and possibly *Ministeria* (23–25), for which there are no published molecular data.

The animals + fungi (opisthokonts; Fig. 2A, node 4) are now a well-established supergroup [reviewed in (8)]. In addition to the combined data (97% aaBP, 100% ntBP, Fig. 1), this group is strongly supported by all large, taxonomically well-sampled molecular data sets, i.e., SSU and LSU rRNA, 70-kD heat shock protein (HSP70), EF-1 α , α -tubulin, β -tubulin, actin, and by the summed maximum likelihood scores of 23 proteins (Fig. 2B) [reviewed in (8)]. These taxa, also including chytrids and probably Choanoflagellates (1–4, 21, 23), share the unique combination of flattened mitochondrial cristae and, when flagellate, the presence of a single basal flagellum on reproductive cells (26).

A grouping of Mycetozoa + the lobose amoeba *Acanthamoeba* (Amoebozoa, Fig. 2A, node 6) is strongly supported by these data (86% aaBP, Fig. 1), by trees of actin (Fig. 2B) and the actin-related proteins ARP2 and ARP3 (27), and by mitochondrial genome similarities in *Dictyostelium* and *Acanthamoeba* (28). Morphologically, these taxa share amoeboid stages with lobose pseudopodia moving in a smooth, nonruptive manner (21, 23). Patterson denotes these taxa the “ramicristates,” on the basis of shared mitochondrial morphology (23).

Combined protein data further place the amoebozoans as the sister group to the opisthokonts (Fig. 2A, node 7). With deletion of the nearby branches of Bangiophyceae and *Cyanophora*, this cluster receives 99% aaBP (85% ntBP, Fig. 1) (29). Thus, these data strongly

place the amoebozoans as a closer sister group to the opisthokonts than all other eukaryotes examined here, with the possible exception of glaucophytes and/or rhodophytes. A close relationship between amoebozoans and opisthokonts is also seen with actin and summed maximum likelihood scores (*Dictyostelium* + opisthokonts), and is suggested by EF-1 α and possibly tubulins [reviewed in (8)]. SSU rRNA data also consistently place the lobosans, at least, very close to opisthokonts (1–4).

One problematic taxon here is the tentatively supported Plantae (Fig. 2A, node 10, and Fig. 1). This group includes the three lines of primary photosynthetic eukaryotes (Rhodophyta, Glaucophyta, and Viridiplantae), all other algae having acquired their plastids second-hand from these [reviewed in (30)]. A holophyletic Plantae, allowing for a single origin of eukaryotic photosynthesis, is well supported by a large body of organelle data [reviewed in (30)]. While confirmation from nuclear gene data is still lacking, especially for glaucophytes, at least two nuclear genes support a red-green plant clade [vacuolar adenosine triphosphatase (V/A-ATPase) and EF-2 (Fig. 2B)], and previous rejection of this group by RPBI is now questioned [reviewed in (10)]. Because rhodophytes and glaucophytes are represented here by only a single taxon each (Fig. 1), increased taxonomic sampling may improve their resolution with these data.

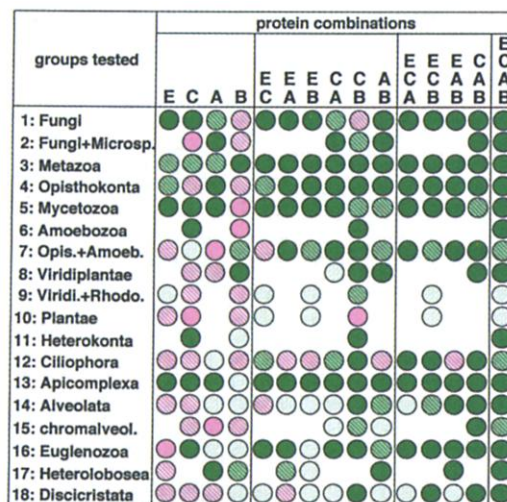
The ciliates + apicomplexans (alveolates, Fig. 2A, node 14) are a widely accepted taxon and are well supported here (86% aaBP, 90% ntBP, Fig. 1), as well as in trees of HSP70, α -tubulin, β -tubulin, SSU rRNA, and LSU rRNA (Fig. 2B); the latter two genes also clearly place the dinoflagellates in this group (1–4). Alveolates possess cortical alveoli or related structures, systems of membrane-bound sacs lying beneath the plasma membrane and performing structural roles or giving rise to external coverings such as pellicles

[ciliates (21)] or thecal plates [dinoflagellates (21)]. The strength of this group in our tree (Fig. 1) is particularly striking, because individual trees of actin and EF-1 α give notoriously poor resolution of these taxa (see above) (15, 16).

The clustering of alveolates + heterokonts (chromalveolates, Fig. 2A, node 15) suggested by these data (61% aaBP, 53% ntBP, Fig. 1; see below) is well supported by trees of HSP70 and SSU rRNA “crown” taxa, and is weakly supported by β -tubulin (Fig. 2B). Although this grouping appears relatively weak in our tree (Fig. 1), the heterokonts are also highly incomplete for these data (Fig. 1), and partitioned analyses suggest that this grouping here may be robust (see below). Cavalier-Smith designates this group the “chromalveolates,” also including in it the haptophyte and cryptophyte algae (31). This grouping would allow for a single gain by secondary (eukaryote-to-eukaryote) endosymbiosis, of all chlorophyll *c*-containing plastids plus the plastid-like organelle of apicomplexans (31). However, there are many fundamental differences between these plastids (30, 31) and, currently, little molecular data on haptophytes and/or cryptophytes to test this question.

Combining data should increase phylogenetic accuracy both by increasing signal and dispersing noise (32) and should uncover the common underlying signal of the data partitions rather than test the relative strengths of conflicts among them (32). Although it is difficult to distinguish true phylogenetic conflict (due to gene paralogy or lateral transfer) from tree reconstruction artifact, the latter is suggested by lack of statistical support for conflicting topologies (33). Furthermore, conflicts that are only weakly supported by a single partition should not lead to strongly supported conclusions (by themselves) in a four-partition analysis. To test for the possible presence and strength of phylogenetic conflict among these data, each par-

Fig. 3. Interactions among data partitions. Phylogenetic support of individual proteins and all their possible combinations (pairwise, three-way, and all four combined) are shown for the taxonomic groupings listed at the left (group numbering as in Fig. 2) (34, 55). Protein combinations analyzed are indicated above by single letters: E = EF-1 α , C = actin, A = α -tubulin, and B = β -tubulin. Accepted groups correspond to nodes found in $\geq 50\%$ of all shortest trees, with the level of bootstrap support indicated by shaded (<50%), striped (50 to 75%), and solid (75 to 100%) green circles (34). Rejected groups are indicated by striped (<50%) and solid (50 to 65%) pink circles, corresponding to the percent aaBP for the most strongly supported alternative grouping including any member(s) of the group in question (34). All taxa missing data for any protein were deleted from relevant analyses; all analyses excluded Diplomonadida and Parabasalia (9).



tion (protein) was analyzed separately, as well as in all possible pairwise and three-way combinations (Fig. 3) (34).

Analyses of individual proteins show that no conflicting groupings are supported by >65% aaBP and most by much less (Fig. 3, columns 1 through 4). Therefore, no strongly supported conflicts exist among these data. Pairwise analyses also show considerable evidence of phylogenetic cooperation among all partitions for most questions (Fig. 3, columns 5 through 10); i.e., most pairwise combinations tend to support the same conclusions. This is further evidence of common underlying histories among all partitions.

Cooperation among partitions is especially clear at the super-taxon level (taxa 4, 7, 14, 15, and 18); most individual proteins reject these groups, but most pairwise combinations support them (Fig. 3). For example, the chromalveolate grouping (node 15) is rejected by all three individual proteins testing it, but all pairwise combinations accept the group at least weakly, and the three proteins combined support it strongly (79 to 80% aaBP) (34) (see note added in proof).

Even paired proteins can give markedly greater resolution. For example, actin and β -tubulin individually support 5 of 17 and 7 of 18, respectively, of all nodes tested, but together find moderate to strong support for 15 of 17 nodes (Fig. 3, columns C, B, and CB). EF-1 α and actin, both notorious for their inability to unify ciliates [see above and (Fig. 2B) (15, 16)], together not only reconstruct this group but give it a moderately strong 71 to 72% aaBP (Fig. 3, line 12, column EC) (34).

Our data (Fig. 1) suggest that the deep-level phylogeny of eukaryotes may be solvable, despite strong predictions to the contrary (6). Furthermore, the resolving power of these data should continue to improve as more of the constituent sequences are completed (35) and taxon sampling is broadened (36). However, all presently available single-gene phylogenies support only a subset of the major taxa found in the combined data tree, and none supports the same subset (Fig. 2B) (37). This suggests that each gene has its own unique set of strengths and weaknesses as a phylogenetic marker, and it is unlikely that any alone will ever be able to strongly, or perhaps even accurately, resolve all deep branches of a universal tree. Nonetheless, our data suggest that many of the apparent conflicts between individual gene trees (Fig. 2B) are relatively superficial (Fig. 3), and we see little evidence here of fundamentally different phylogenetic histories [as expected if lateral transfer affected these genes (38)].

The single most critical question unanswered by these data is the position of the root of the tree (Fig. 1). Data sets with close archaeal or bacterial homologs are needed to address this most fundamental question.

Note added in proof: Recent evidence suggests that the *Porphyra* (Bangioophyta) btub-2 used here is from an oomycete contaminant, the highly divergent btub-1 being the true red algal gene (56). Consistent with this, substituting btub-1 for btub-2 increases chromalveolate support to 72% aaBP (Fig. 1). The only other change seen is a weak attraction of the now very long Bangioophyta branch to the nearby Amoebozoa, further destabilizing the Plantae clade (57).

References and Notes

1. Y. Van de Peer, R. de Wachter, *J. Mol. Evol.* **45**, 619 (1997).
2. T. Cavalier-Smith, E. E. Chao, *J. Mol. Evol.* **43**, 551 (1996).
3. S. Kumar, A. Rzhetsky, *J. Mol. Evol.* **42**, 183 (1996).
4. M. L. Sogin, *Curr. Opin. Genet. Dev.* **7**, 792 (1997).
5. A. H. Knoll, *Science* **256**, 622 (1992).
6. H. Philippe et al., *Proc. R. Soc. London Ser. B* **267**, 1213 (2000).
7. D. M. Hillis, J. P. Huelsenbeck, C. W. Cunningham, *Science* **264**, 671 (1994).
8. S. L. Baldauf, *Am. Nat.* **154**, S178 (1999).
9. Diplomonads, parabasalids, and entamoebids, the only strong phylogenetic conflicts among these data, were excluded from most analyses (see below). These taxa branch with animals + fungi with tubulins; among the deepest protists with EF-1 α and actin (8).
10. D. Moreira, H. Le Guyader, H. Philippe, *Nature* **205**, 69 (2000).
11. Current implementations of protein maximum likelihood score missing data as gap characters (39, 40). Distance methods tend to radically misplace highly incomplete taxa (S. L. Baldauf, unpublished data).
12. D. L. Swofford, *PAUP: Phylogenetic Analysis Using Parsimony and Other Methods*, beta version 1 (Sinauer, Sunderland, MA, in press).
13. J. Felsenstein, G. A. Churchill, *Mol. Biol. Evol.* **13**, 93 (1996).
14. D. M. Hillis, J. J. Bull, *Syst. Biol.* **42**, 182 (1993).
15. D. Moreira, H. Le Guyader, H. Philippe, *Mol. Biol. Evol.* **16**, 234 (1999).
16. G. Drouin, M. Moniz de Sa, M. Zucker, *J. Mol. Evol.* **41**, 841 (1995).
17. Y. Van de Peer, A. B. Abdelghani, A. Meyer, *Gene* **246**, 1 (2000).
18. A. J. Roger, thesis, Dalhousie University, Halifax, Canada (1996).
19. P. De Rijk, Y. Van de Peer, I. Van den Broeck, R. De Wachter, *J. Mol. Evol.* **41**, 366 (1995).
20. S. L. Baldauf, W. F. Doolittle, *Proc. Natl. Acad. Sci. U.S.A.* **94**, 12007 (1997).
21. K. Hausmann, N. Hulsman, *Protozoology* (Thieme, New York, 1996).
22. P. J. Keeling, J. A. Deane, G. I. McFadden, *J. Eukaryot. Microbiol.* **45**, 561 (1998).
23. D. J. Patterson, *Am. Nat.* **154**, S96 (1999).
24. T. Cavalier-Smith, *Biol. Rev.* **73**, 203 (1998).
25. C. J. O'Kelly, T. A. Nerad, *J. Eukaryot. Microbiol.* **46**, 522 (1999).
26. T. Cavalier-Smith, in *Evolutionary Biology of Fungi*, A. D. M. Rayner, C. M. Brasier, D. Moore, Eds. (Cambridge Univ. Press, Cambridge, 1987), pp. 339–353.
27. J. F. Kelleher, S. J. Atkinson, T. D. Pollard, *J. Cell Biol.* **131**, 385 (1995).
28. M. Iwamoto, M. Pi, M. Kurihara, T. Morio, Y. Tanaka, *Curr. Genet.* **33**, 304 (1998).
29. Nucleotide-level analyses of these data seem particularly sensitive to highly incomplete data (*Acanthamoeba*) and unstable branches (Bangioophyceae and Cyanophora); inclusion of these taxa markedly lower ntBPs for several distantly related nodes.
30. S. E. Douglas, *Curr. Opin. Genet. Dev.* **8**, 655 (1998).
31. T. Cavalier-Smith, *J. Eukaryot. Microbiol.* **46**, 347 (1999).
32. A. de Queiroz, M. J. Donoghue, J. Kim, *Annu. Rev. Ecol. Syst.* **26**, 657 (1995).
33. J. Sullivan, *Syst. Biol.* **45**, 375 (1996).

34. Supplementary material is available at www.sciencemag.org/feature/data/1047151.shl
35. J. J. Weins, *Syst. Biol.* **47**, 625 (1998).
36. D. M. Hillis, *Syst. Biol.* **47**, 3 (1998).
37. T. M. Embley, R. P. Hirt, *Curr. Opin. Genet. Dev.* **8**, 624 (1998).
38. W. F. Doolittle, *Science* **284**, 2124 (1999).
39. J. Adachi, M. Hasegawa, *Comput. Sci. Monogr.* **28**, 1 (1996).
40. K. Strimmer, A. von Haeseler, *Proc. Natl. Acad. Sci. U.S.A.* **94**, 6815 (1997).
41. J. Felsenstein, *PHYLIP (Phylogeny Inference Package)*, version 3.5c (Department of Genetics, University of Washington, Seattle, WA, 1993).
42. I. Wenk-Siefert, thesis, Universitat Zurich, Zurich, Switzerland (1994).
43. W. P. Maddison, D. R. Maddison, *MacClade: Analysis of Phylogeny and Character Evolution*, version 3 (Sinauer, Sunderland, MA, 1992).
44. Sequences were aligned by eye, because length variations are small and rare. Gaps and any adjacent ambiguous alignment were deleted, as were 5' and 3' termini (missing in PCR-generated sequences). Monophyly of peripheral clusters was tested with all available sequences by 100 bootstrap replicates of PAM 250-corrected neighbor-joining distances (47). These clusters were then trimmed to favor short terminal branches and taxonomic breadth. The final data set includes 834 parsimony-informative sites and is available from SLB on request. Sequencing of *Acrasis* EF-1 α and *Nosema* β -tubulin (18) and of *Polysphondylium* and *Acytostelium* α - and β -tubulin and *Acrasis* β -tubulin (42) have been described (GenBank accession numbers AF190771-2 and AF276942-7). All final analyses were derived from PAUP* 4.0b2 with default settings (12) unless otherwise noted. Amino acid parsimony analyses utilized optimal tree searches of 10,000 rounds of random sequence addition and 10,000 bootstrap replicates. Branch lengths were averaged over three optimization strategies [acctran, deltran, and minf (43)]. Maximum likelihood analyses of second codon-position nucleotides utilized the F84 (13) and GTR+I+G (34) substitution models and 100 (Fig. 1) or 500 (34) bootstrap replicates. Although the GTR+I+G model gave the closest fit to these data, both models gave very similar results (34).
45. The tree has a retention index of 0.6255; rescaled consistency index of 0.3380. One added tree island was found at 5060 steps placing *Cyanophora* as outgroup to animals + fungi and Bangioophyceae as outgroup to Amoebozoa. Phylogeny of animals is not reliably resolved here due to their complex multigene families for all proteins except EF-1 α (8).
46. Considerable data place diplomonads and parabasalids among the earliest diverging eukaryotes (37). However, their placement in this tree is highly tentative due to strong conflict among these proteins on this issue (8, 9) and the lack of actin data. Therefore, these taxa are appended to the final tree on the basis of separate analyses including all taxa, which place them, with ~50% aaBP, as shown or as the outgroup to opisthokonts.
47. Terminal branch lengths were increased proportionally for taxa missing >25% of the data (e.g., the branch length of a taxon missing one complete gene would be multiplied by 4/3). Internal branches, where all subsequently arising taxa have the same percentage of missing data, were likewise increased.
48. G. Van der Auwera, C. J. B. Hofmann, P. De Rijk, R. De Wachter, *Mol. Phylogenet. Evol.* **10**, 333 (1998).
49. E. Hilario, J. P. Gogarten, *J. Mol. Evol.* **46**, 703 (1998).
50. A. Germot, H. Philippe, *J. Eukaryot. Microbiol.* **46**, 116 (1999).
51. B. F. Lang, E. Seif, M. W. Gray, C. J. O'Kelly, G. Burger, *J. Eukaryot. Microbiol.* **46**, 320 (1999).
52. R. P. Hirt et al., *Proc. Natl. Acad. Sci. U.S.A.* **96**, 580 (1999).
53. D. Bhattacharya, J. Ehling, *Arch. Protistenkd.* **145**, 155 (1993).
54. P. J. Keeling, W. F. Doolittle, *Mol. Biol. Evol.* **13**, 1297 (1996).
55. Amino acid sequences were analyzed as described (44) except that optimal tree searches used 100 rounds of random sequence addition and bootstrap analyses used 1000 replicates of one round of ran-

dom addition with a maximum tree-ceiling of 500. Taxa were excluded from analyses of partitions for which they had missing data.
 56. R. MacKay, personal communication.
 57. S. L. Baldauf, A. J. Roger, unpublished data.

58. We thank M. E. Holder of the University of Houston High Performance Computing Center for help with likelihood analyses, Y. van de Peer for useful discussions, and especially J. Felsenstein for the original suggestion. Supported in part by a National Sciences and Engineer-

ing Council of Canada (NSERC) grant 227085 to A.J.R. and by a Medical Research Council of Canada (MRC) grant MT4467 to W.F.D.

17 November 1999; accepted 26 September 2000

Recovery and Management Options for Spring/Summer Chinook Salmon in the Columbia River Basin

Peter Kareiva,¹ Michelle Marvier,² Michelle McClure^{1*}

Construction of four dams on the lower Snake River (in northwestern United States) between 1961 and 1975 altered salmon spawning habitat, elevated smolt and adult migration mortality, and contributed to severe declines of Snake River salmon populations. By applying a matrix model to long-term population data, we found that (i) dam passage improvements have dramatically mitigated direct mortality associated with dams; (ii) even if main stem survival were elevated to 100%, Snake River spring/summer chinook salmon (*Oncorhynchus tshawytscha*) would probably continue to decline toward extinction; and (iii) modest reductions in first-year mortality or estuarine mortality would reverse current population declines.

Dams in the Columbia River Basin of North America almost certainly contributed to severe declines in wild salmon runs (1). Some dams in this basin, such as the Hell's Canyon Dam, completely blocked salmon passage, eliminating much spawning habitat (2). Other dams allow fish passage, but turbines, predation in reservoirs, and other alterations in the migration corridor presumably increase salmon mortality (1). Ecological problems associated with dams are widespread (1) and are leading to societal questions weighing the benefits of dams against their costs to depleted fish populations. The most dramatic decision yet faced involves four hydroelectric dams on the lower Snake River.

Salmonid evolutionarily significant units (ESUs) represent genetically distinct collections of populations (3). In western North America, 24 salmonid ESUs are listed under the Endangered Species Act; 12 of these are in the Columbia River Basin and four must pass the four lower Snake River dams. The U.S. Army Corps of Engineers is currently considering removing these dams to recover Snake River salmon (4). Although most scientists agree that dam removal will help salmon (5), it is not known how much benefit would be derived from this action or whether alternative modifications of fish passage could lead to population recovery.

¹National Marine Fisheries Service, Northwest Fisheries Science Center, 2725 Montlake Boulevard East, Seattle, WA 98112, USA. ²Department of Biology, Santa Clara University, Santa Clara, CA 95053, USA.

*To whom correspondence should be addressed. E-mail: Michelle.McClure@noaa.gov

We used an age-structured matrix model (6, 7) for Snake River spring/summer (SRSS) chinook salmon to describe the current situation and explore the demographic effects of reducing mortality at different life stages. Seven index stocks of SRSS chinook salmon have been intensively monitored since the late 1950s (8); all are declining (Fig. 1 and Web fig. 1) (9), with current spawning populations averaging less than 10% of their 1950 levels (8). Using age-specific spawner data, we estimated demographic projection matrices for these index stocks (Table 1). The matrices isolate survival during upriver and downriver migration from survival in other life stages, allowing direct examination of the effect of mortality during in-river migration on population growth. These simple matrix models are density-independent; we found little evidence supporting a density-dependent model (9).

We used data for 1990–1994 brood years to estimate parameters for matrices for all index stocks (Table 2), restricting analyses to recent years because these stocks have suffered progressively declining productivity. We thus examined a worst case scenario, taking a precautionary approach to the evaluation of endangered species. The dominant eigenvalues of these matrices indicate the long-term annual rates of population change (assuming that demographic rates remain constant) and all are substantially less than one.

We used these matrices to determine the effect of eliminating all migration mortality except for a small tribal harvest. Although perfect survival during in-river migration is unobtainable, it is a useful numerical exper-

iment because one goal of both dam breaching and modification of intact dams is to reduce in-river migration mortality. Remarkably, even if every juvenile fish that migrated downstream survived to the mouth of the Columbia, and every returning unharvested adult fish survived to reach the spawning grounds, the index stocks would continue to decline (Fig. 2). Thus, management aimed solely at improving in-river migration survival cannot reverse the SRSS chinook decline.

We also tested the effectiveness of three past management actions: (i) reductions of harvest rates, from approximately 50% in the 1960s to less than 10% in the 1990s (8); (ii) engineering improvements that increased juvenile downstream migration survival rates from approximately 10% just after the last turbines were installed to 40 to 60% in most recent years (10); and (iii) the transportation of approximately 70% of juvenile fish from the uppermost dams to below Bonneville Dam, the lowest dam on the Columbia River (5). If such improvements had not been made, the rates of decline would likely have been 50 to 60% annually (Fig. 3), and spring/summer chinook salmon might well have already disappeared from the Snake River. Hence, past management actions have reduced in-river mortality but have not reversed population declines.

Finally, we tested whether improved survival at other life stages could reverse the population declines. Choosing the matrix with the median dominant eigenvalue (Poverty Flat) as a benchmark, we calculated combinations of first-year survival (s_1) and early ocean/estuarine survival (s_e) values that give a dominant eigenvalue of 1.0 [a steady-state population in a deterministic world (Fig. 4)]. We neglected adult mortality because ocean harvest is negligible on these stocks, and

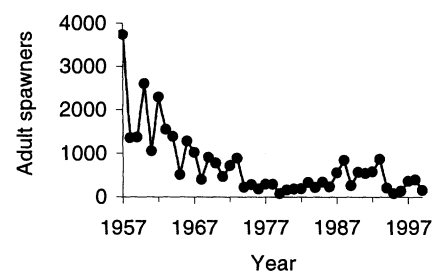


Fig. 1. Total adult (4- and 5-year-old) spawners from 1957–1999 in Poverty Flat index stock of SRSS chinook salmon. Data are based on redd (nest) counts made along a standardized segment of each stream and extrapolated to the full length (8). Poverty Flat is presented because it exhibited the median predicted rate of population growth (9).